Integrated Spectral Image Registration Protocol for Enhanced Land Pollution Assessment and Management: Bridging Satellite and Drone Data for High-Resolution Mapping

Natsuo Okada[1], Hisatoshi Toriya[2], Angesom Gebretsadik[1,4], Takahiko Arima[3], Yoko Ohtomo[3] and Youhei Kawamura[3]

[1] Division of Sustainable Resources Engineering, Graduate School of Engineering, Hokkaido University, Japan: natsu0807chi@gmail.com (N.O.); angstg2007@gmail.com (A.G.)

[2] Graduate School of International Resource Sciences Department of Earth Resource Engineering and Environmental Science, Akita University, Japan: toriya@gipc.akita-u.ac.jp (H.T)

[3] Division of Sustainable Resources Engineering, Faculty of Engineering, Hokkaido University, Kita-13, Nishi-8, Sapporo 060-8628, Japan: kawamura@eng.hokudai.ac.jp (Y.K.); ohtomoy@eng.hokudai.ac.jp (Y.O.); takahiko_arima@eng.hokudai.ac.jp (T.A.).

[4] Department of Mining Engineering, Aksum University, Aksum, Tigray,7080, Ethiopia: angstg2007@gmail.com (A.G.)

ABSTRACT: A satellite equipped with a spectroscopy camera is a valuable tool for examining land pollution caused by mine waste across a large region. Due to the limited resolution of spectral images, merging them with high-resolution images obtained at lower altitudes can improve local resolution without producing pseudo-data. In order to produce high-resolution spectrum maps from spectral data gathered from satellite and drone imagery shot at various altitudes, an image registration procedure was devised in this study. The establishment of this protocol will facilitate the development of more precise land pollution discovery techniques and aid in the integration of various altitude data, which has not been fully utilized up to this point altitudes. The development of novel methods for sophisticated image registration and the system's implementation through field research and lab testing are the two primary objectives of this project. We suggested a process and technique for spectral image registration in the first section. In the second section, spectral images captured at different elevations at the mine site were used to test the image registration using the suggesting method. Consequently, spectral image registration algorithms for different altitudes and high-resolution spectral maps were established.

Keywords: Image registration; Remote sensing; GIS; Hyperspectral imaging; Digital Twin

Abbreviations.

HSI- Hyperspectral imaging

MSI- Multispectral imaging

SURF- Speeded Up Robust Features

UAV- Unmanned Aerial Vehicle

1. Introduction

Mining development is widely recognized for its propensity to induce a multitude of environmental issues [1], [2], [3] due to its substantial modification of the surrounding ecosystem. Specifically, the heavy metal minerals that are left unused and exposed on the ground due to mining activities undergo oxidation when they encounter air. This process causes them to dissolve in rainwater and groundwater, leading to pollution of the soil [4]. The utilization of remote sensing technology for detection purposes [5] has great potential due to its ability to cover a vast expanse of soil contamination locations. Given that the pollution consists of mineral-based heavy metal contamination, it may be suitable to employ approaches commonly utilized in the field of resource exploitation.

It is widely recognized that each mineral possesses a unique absorption spectral band, and spectroscopy can be employed to distinguish several mineral species by analyzing spectral data [6], [7], [8], [9]. The analysis of data obtained from a spectral camera mounted on a satellite is used to assess the spatial distribution of minerals in remote sensing resource exploitation. The utilization of satellite spectral data has been on the rise due to recent notable progress in analysis technology, such as the introduction of deep learning-based methods for mineral identification, and the decreasing cost of satellite launches, which has made data collection more accessible. While there have been advancements in data processing and access, limitations in hardware prevent the examination of a wide range of data in the spectrum, and there is still a need for improvement in data quality. The main characteristics of spectral data are its spatial resolution and spectral resolution. Nevertheless, in the case of most spectrum cameras, there is a correlation between both values, implying that increasing one parameter would invariably result in a decrease in the other. As a result, achieving a significant improvement is unlikely [10]. Therefore, satellite spectral pictures necessitate enhanced spatial resolution.

Over the past few years, there has been a significant rise in the acquisition of aerial spectrum data globally. This can be attributed to advancements in drone, aircraft, and satellite technology, as well as the decrease in their cost. Nevertheless, the lack of success in establishing a connection between these data can be attributed to variations in altitude and the diverse locations from which the data was collected. In this study, our objective was to generate high-resolution spectrum data by overlaying spectral data groups gathered from different altitudes, such as satellites, aircraft, and drones, without introducing any artificial data. The uniqueness of this study is that it does not create spectra, therefore enabling the user to directly access the unprocessed data. Various techniques have previously been suggested to enhance the spatial resolution of spectral data. Our objective was to generate spectrum data with a high level of detail without resorting to the use of artificially created data. Additionally, we aimed to analyze a sporadically gathered collection of spectral data on a digital twin platform.

There is a disparity between satellite and drone data in terms of their spatial coverage. Therefore, our method involves conducting a first extensive survey of a large geographic area utilizing satellite data. This survey is not meant to be comprehensive, but rather to determine the precise area of contamination. Following the initial drone surveys, subsequent aerial inspections will be carried out in the presumed polluted regions to perform a more comprehensive examination. Our goal for the future is to create a data twin platform to accommodate the growing volume of data.

The utilization of digital twin technology [11] is essential in our approach, as it acts as the fundamental foundation for the integration and analysis of data. Digital twins enable the generation of virtual replicas of actual environments and processes, allowing for real-time prediction, optimization, monitoring, and management. In the context of mining and environmental monitoring, digital twins provide a strong framework for integrating spectral data from several sources and facilitating complete analysis across various sections. Our research employs sophisticated image registration algorithms to enhance the spatial resolution of spectral pictures and make more informed decisions in mining and environmental management by utilizing digital twin technologies. This study presents a novel spectral image registration technique to enhance spatial resolution on the platform. Additionally, a digital platform protocol is proposed for integrating infrequently processed huge data sets.

1.1. Literature review

The low resolution of image data obtained from satellites, particularly hyperspectral data, has prompted a number of studies to investigate methods of improving this resolution. According to Yokoya, techniques for increasing the resolution of hyperspectral images can be classified into four categories: hyperspectral super resolution (multiple images, single image), subpixel mapping (or super resolution mapping), hyperspectral sharpening, and hyper- and multispectral data fusion [12]. It is important to note that the definitions of these terms are not entirely clear. For instance, some authors categorize super-resolution or pan-sharpening as a distinct form of data fusion, whereas others view high-resolution hyperspectral data as an example of "super resolution". Super-resolution constitutes a specific form of data fusion.

1.1.1. Super resolution

According to Yokoya, two distinct forms of super-resolution have been identified: 1. Multiple-frame super-resolution that reconstructs a high-resolution image from multiple low-resolution images, and 2. Learning based super-resolution [12]. Super resolution methods have been proposed, including those using linear deterministic models [13] and deep learning-based methods [14], [15], [16], [17].

1.1.2. Sub pixel mapping

Sub-pixel mapping is a technique that converts fractional images into a higher-resolution classification map, thereby enabling the acquisition of the spatial distribution of various classes at the sub-pixel scale [18]. Typical algorithms known include Attraction Model, Pixel Swapping Algorithm, Genetic Algorithms, and Hopfield Neural Network [19]. Recently, methods employing CNN models have also been proposed [20].

1.1.3. Pan sharpening

Pan-sharpening is the process of combining a low-resolution spectral image with a high-resolution panchromatic (PAN) image to create a high-resolution spectral image [21]. Pan sharpening algorithms can be broadly classified into three categories (Component Substitution: CS, MultiResolution Analysis: MRA, and Sparse representation) [22], [23]. The CS (or projection substitution) has many derived families such as IHA, PCA, and GS. Traditionally, CS has been mainly studied for multispectral data, but with the rise of hyperspectral data, pan-sharpening studies have been conducted for these data [24]. The second method, MRA, has several methods and have been proposed, including HPF, HPM, Indusion, MTF-GLP-CBD, ATWT, and others.

1.1.4. Hyper-Multi spectral data fusion

In contrast to the process of pan sharpening, the high-resolution image incorporates spectral information, thereby facilitating more precise reconstruction of the spectral signal and can be classified into two categories: extensions of pan sharpening and approaches based on subspace methods [12]. A number of techniques have been put forth to address this data-fusion issue, drawing upon disparate theoretical frameworks. These include CS, MRA, spectral unmixing, and Bayesian probability [25].

In comparison, the endeavours to enhance the resolution of hyperspectral, as explained above, result in the generation of pseudo-spectra from the original data. Although numerous innovative methodologies have been proposed, an integrated approach to image registration that does not modify the raw data has yet to be studied.

2. Methodology and material used.

2.1. Protocol for registering spectral images utilizing spectral data from various altitudes.

2.1.1. Procedure the spectral image registration protocol

Our process starts by obtaining spectrum data from several sources, such as in-situ hyperspectral imaging, drone multispectral imaging, and satellite multispectral imaging. The spectral pictures acquired from these sources display discrepancies in spatial resolution and perspective as a result of disparities in altitude and imaging conditions. In order to tackle this difficulty, we utilize a multi-step picture registration procedure, as seen in the provided in Figure 1. This procedure entails rectifying projective distortion in spectral data, generating top-down perspective transformations, and aligning spectral images by extracting and selecting feature points. Our technology seeks to enhance spatial resolution and facilitate precise analysis of mining and environmental data by matching spectral data acquired from various elevations in a systematic manner.

The integration of data obtained from disparate altitudes and disparate aerial survey methodologies offers the following advantages. Firstly, data obtained from satellites encompasses a distance of several hundred kilometers from the camera to the object being imaged, with ground surface resolution being limited to a few tens of meters. As a result, a comprehensive examination of the ground surface is not feasible; however, it is possible to conduct a preliminary investigation across a broad region. The ground resolution of spectral data acquired from an altitude of tens of meters above the surface, such as by a drone, is several centimeters, which is considerably higher than that of satellite data. While this method is not optimal for surveying extensive areas, it can be utilized to survey specific regions with high precision. Data obtained from aircraft at an altitude between that of drones and satellites play a pivotal role in image registration. The resolution of satellite data differs significantly from that of drone data, rendering automatic feature point extraction impractical. However, by incorporating data of intermediate resolution acquired from intermediate altitudes into the image registration process, mutual registration with satellite and drone data becomes feasible.

The procedure for image registration for spectrum data obtained at various altitudes is shown in this flowchart. Initial spectral data sources for the flowchart include "In-situ HSI," "Drone MSI," "Satellite MSI," and "Drone Orthomosaic." It then moves on to a decision-making procedure to determine whether projection distortion is present. It goes to "Pseudo-bird's-eye view image" if there is distortion, and to "RGB transformation" and "Detect SURF features" if there isn't. A second decision point ascertains whether the feature point extraction technique SURF (Speeded Up Robust Features) can detect features; if it can, it moves on to "Control Points Selection"; if not, it uses "2-D projective transformation." A digital twin model is also created using drone imagery that is acquired from spectral data sources. Finally, the resulting digital twin is used for altitude-varying spectral image registration.

Table 1 displays the spectral data that need to be aligned. The orthomosaic data is generated when constructing a digital twin from drone images.

Table 1 Spectral data set.

Name	Type of spectral	Camera	Altitudes	Bands Number	Wavelength (nm)
In-situ	HSI	Specim IQ	1 m	204	400 ~ 1000
Drone	MSI	P4 Multispectral	50 m	5 (Blue, Green, Red, RE and NIR)	450 ~ 840
Orthomosaic	MSI	P4 Multispectral	50+ m	5 (Blue, Green, Red, RE and NIR)	450 ~ 840
Satellite	MSI	AVNIR-2_1B1	690 km	4 (Blue, Green, Red and NIR)	420 ~ 890

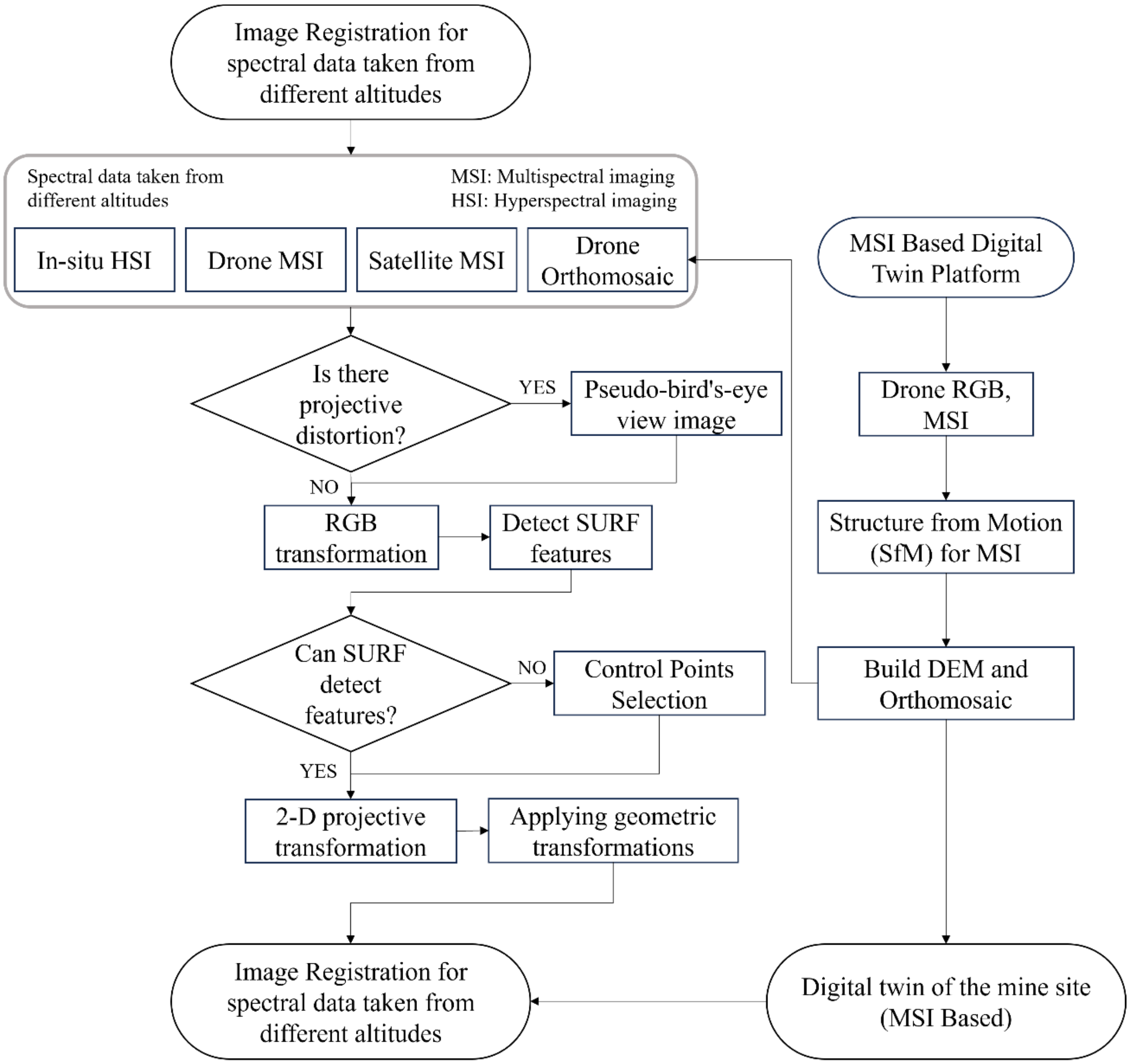

Figure 1 Flowchart of the proposing protocol.

2.2. Digital Twin platform

The application of digital twin technology, which is a virtual version of a physical thing or process, is expanding across a number of industries, including smart cities, automotive, industrial, and medical [26]. It is a transformational tool in the design and operation of cyber-physical intelligent systems, enabling real-time prediction, optimization, monitoring, and control [27]. Modeling and simulation, which assist stakeholders throughout the lifecycle of the system or item, are the fundamental components of the technology [28]. Conceptual diagram is shown in Figure 2. Even though spectral data is being collected at an increasing rate globally, there is still a lack of coordination among the data, which leads to irregular data processing. We built a 3D platform to facilitate the easy collecting and analysis of spectrum data from field surveys and interior experiments. RGB photos of the mine collected by the UAV are analyzed by Structure from Motion to create 3D data, which serves as the foundation model for the digital twin.

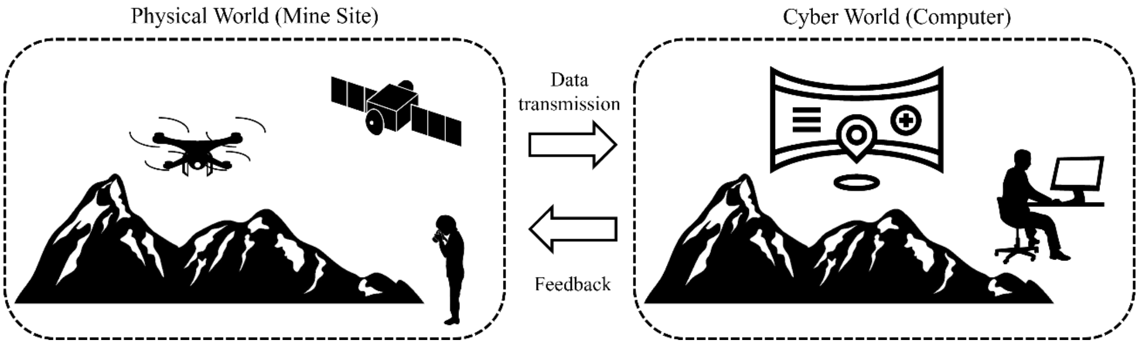

Figure 2 Digital Twin for mining.

2.3. Projective distortion of spectral data

As low-altitude spectral data, an overhead view image of the Mine's surface was captured using a hyperspectral camera (Specim IQ) mounted on a tripod. The oblique direction of an image taken from a tripod, as depicted in Figure 3, results in projective distortion, which reduces the resolution of the image from the front to the back. It is required to carry out a projective transformation (bird's-eye view image transformation) as if the image was taken from a vertical direction in order to correctly image registration with a spectral image of a different altitude taken from a vertical direction (Virtual Top View) [29], [30]. This study performed the bird's-eye view transformation on all band images and approximated the transformation matrix based on the camera's shooting angle.

The process for bird's eye view image transformation is depicted in Figure 3. The internal parameter matrix *K* of the camera, the corresponding rotation matrices *R* and *R′*, and the 3D positions *c* and *c′*, respectively, are used to generate the perspective projection matrix *P* of the shooting camera and the perspective projection matrix *P′* of the translated and rotated bird's-eye view camera.

$$P = K[R| - Rc] \tag{3}$$

$$P' = K[R'| - R'c''] \tag{4}$$

can be expressed as the rotation matrices *R* and *R′* are calculated based on the values of the acceleration sensor mounted on the mobile terminal used for photography. If the coordinate transformation matrix (rotation matrix) by rotation from *R* to *R′* is defined as *ΔR*, the two-dimensional projection transformation matrix *HΔR*, which projects any point in the captured image by the rotation transformation *ΔR*, can be expressed as follows from equations (3) and (4),

$$H_{\Delta R} = K(\Delta R)K^{-1} \tag{5}$$

and can be obtained from the gravity information of the acceleration sensor. On the other hand, the parallel shift vector Δc from c to c' is,

$$\Delta c = c' - c \tag{6}$$

Δc depends on the spatial resolution of the generated pseudo-overhead image. Usually, Δc is set so that the spatial resolution of the low-altitude image and the image resolution of the pseudo-overhead image are equivalent in order to improve the efficiency of the correspondence point search process. If $H\Delta c$ is a 2-dimensional projective transformation matrix that projects an arbitrary point in the image according to the parallel shift Δc, then the 2-dimensional projective transformation matrix H_1 that projects the image taken by the user viewpoint camera to the pseudo-bird's-eye view image from the bird's-eye view camera is,

$$H_1 = H_{\Delta c} H_{\Delta R} \tag{7}$$

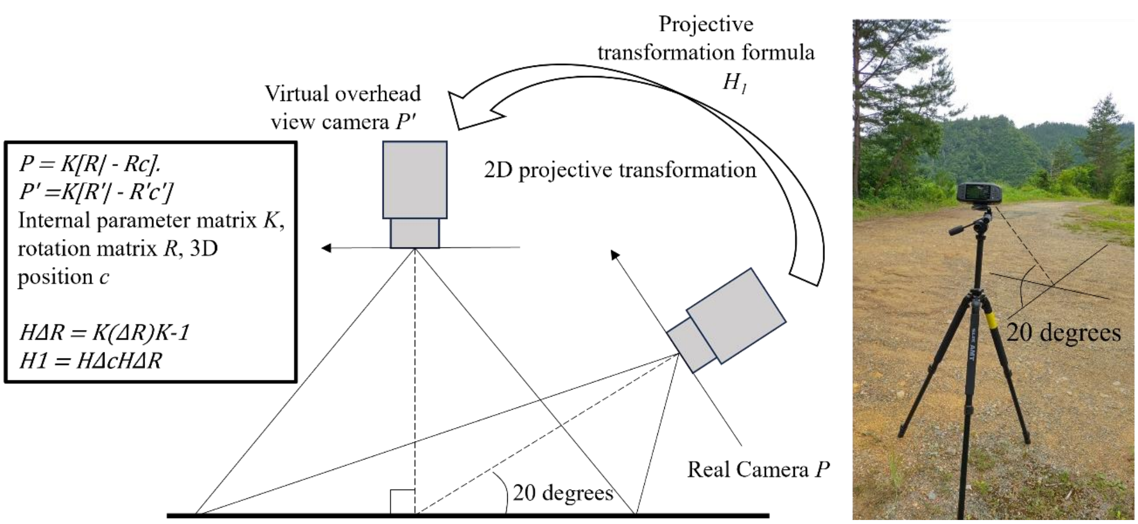

Figure 3 Bird's eye transformation.

2.4. Spectral image registration

In this study, spectral images with variable spatial resolution acquired from different altitudes are aligned to improve the local spatial resolution of low-spatial-resolution spectral images. Figure 4 illustrates the alignment procedure. The high-spatial-resolution spectral imagery obtained over a restricted region (spectral image taken from a lower altitude than the Fixed image at the research site) was defined as the Move image, while the low-spatial-resolution spectral image taken over a vast area was designated as the Fixed image. From them, RGB images were constructed from data cubes, and between the matched images, feature point extraction was carried out by selecting control points. After that, image registration was carried out using the subsequent procedures: 1. Posture estimation; 2. Estimation of transformation models; and 3. Resampling and transformation. In order to preserve the spatial resolution of the image collected from lower altitudes, image registration was done to match the spectral image taken from higher altitudes. Although it is challenging to automatically extract feature points due to the considerable differences in data resolution that occur with altitude differences, the alignment can be accomplished manually by setting control points. Because the spectral imagery utilized in this investigation had a significant variance in altitude, feature points were chosen and aligned manually.

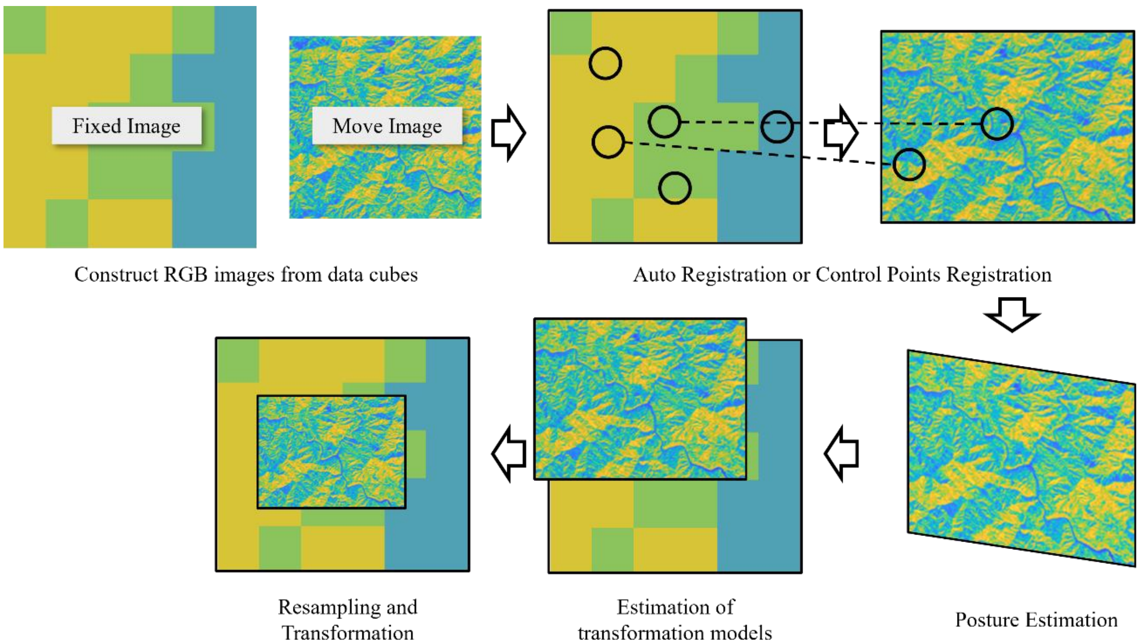

Figure 4 Schematic diagram of image registration.

2.5. Bird' eye transformation process

This chapter discusses the shortcomings of conventional feature point extraction algorithms, such SURF, when dealing with data that has large variations in surface resolution or altitude. An interactive feature point extraction method is presented to address this, in which control points are chosen by hand. With the specified control points as a basis, we estimated a similarity transformation model. By using the calculated geometric transformation to map the places of the output image to corresponding positions in the input image, image registration is accomplished. When the centers of pixels are not aligned, interpolation is utilized. Lastly, to ensure alignment across all band photos, the same geometric transformation is done to register images in other spectral bands. The process is shown in Figure 5.

a) Feature point search

In image processing and computer vision jobs, feature point extraction algorithms like SURF (Speeded-Up Robust Features) are typically helpful. However, as handled in this work, they were unable to be adjusted to data with significant altitude changes, or major surface resolution differences. To be able to replace it, we interactively extracted feature points to serve as control points. The corresponding points between the Fixed and Move images were selected by opening an interactive selection tool. We chose at least four pairs of control points and determined the coordinates of valid move and fixed control point pairs to approximate the projective transformation to control points.

b) Transformation model

We estimated the geometric transformation after looking for the feature points. Since the moving image's geometry remained unchanged in this instance due to the combined effects of translation, rotation, and isotropic scaling, a similarity transformation was utilized as the transformation model. The matrices *X* and *Y* after rotation are then given by the following equations if the rotation is θ, in accordance with the geometric transformation.

$$\begin{pmatrix} X \\ Y \\ 1 \end{pmatrix} = \begin{pmatrix} cos\theta & -sin\theta & 0 \\ sin\theta & cos\theta & 0 \\ 0 & 0 & 1 \end{pmatrix} \begin{pmatrix} x \\ y \\ 1 \end{pmatrix} \tag{8}$$

Also, for isotropic scaling, if we scale by a factor of S_x in the x direction and by a factor of S_y in the *y* direction, the matrices *X* and *Y* after scaling are the lower

$$\begin{pmatrix} X \\ Y \\ 1 \end{pmatrix} = \begin{pmatrix} S_x & 0 & 0 \\ 0 & S_y & 0 \\ 0 & 0 & 1 \end{pmatrix} \begin{pmatrix} x \\ y \\ 1 \end{pmatrix} \tag{9}$$

c) Image Registration

Applying the image's computed geometric transformation allowed for image registration. Mapping the locations of the output image to the corresponding positions in the input image yielded the values of the pixels in the output image. The output pixel value was determined using interpolation within the input image in cases where the center of a pixel in the output image did not match the center of a pixel in the input image.

d) Image registration was performed on other spectral bands

To overlay all band imagery on the same coordinates, the image's geometric transformation was applied to the remaining spectral bands.

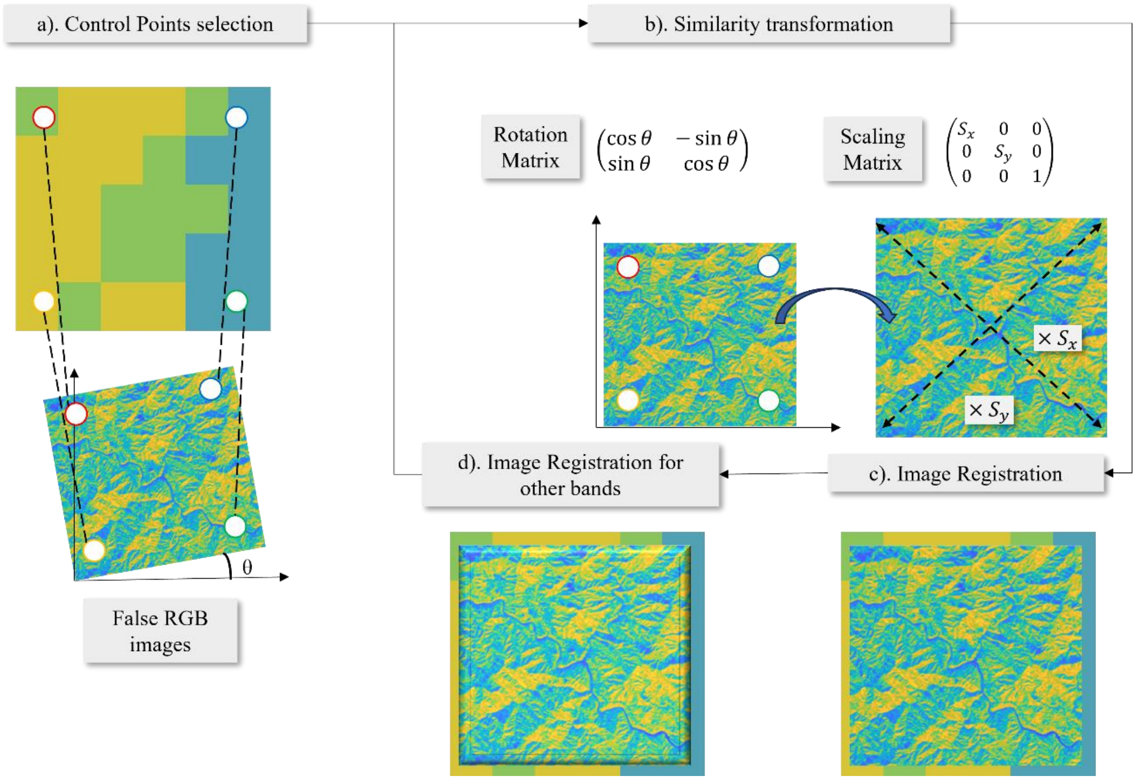

Figure 5 A schematic diagram of control points selection and image registration.

2.6. Overall process

Figure 6 illustrates a process for resolving low spatial resolution by employing spectrum information gathered from drone and satellite sources. First, a range of spectral images obtained at different altitudes are displayed, comprising in-situ (Specim IQ) HSI, drone (DJI P4), and satellite (AVNIR-2) MSI. Utilizing spectral images from lower altitudes improve the situation because of the limited spatial resolution of spectral images obtained from satellites. To improve the presentation of spatial data, image registration of the gathered data is then carried out on a digital twin platform, fusing real-world data with virtual technology. Features point extraction and selection are among the procedures involved in image registration. By putting these methods into practice, spatial data visualization is improved since high-resolution spectral imagery can be seen even when the map is magnified.

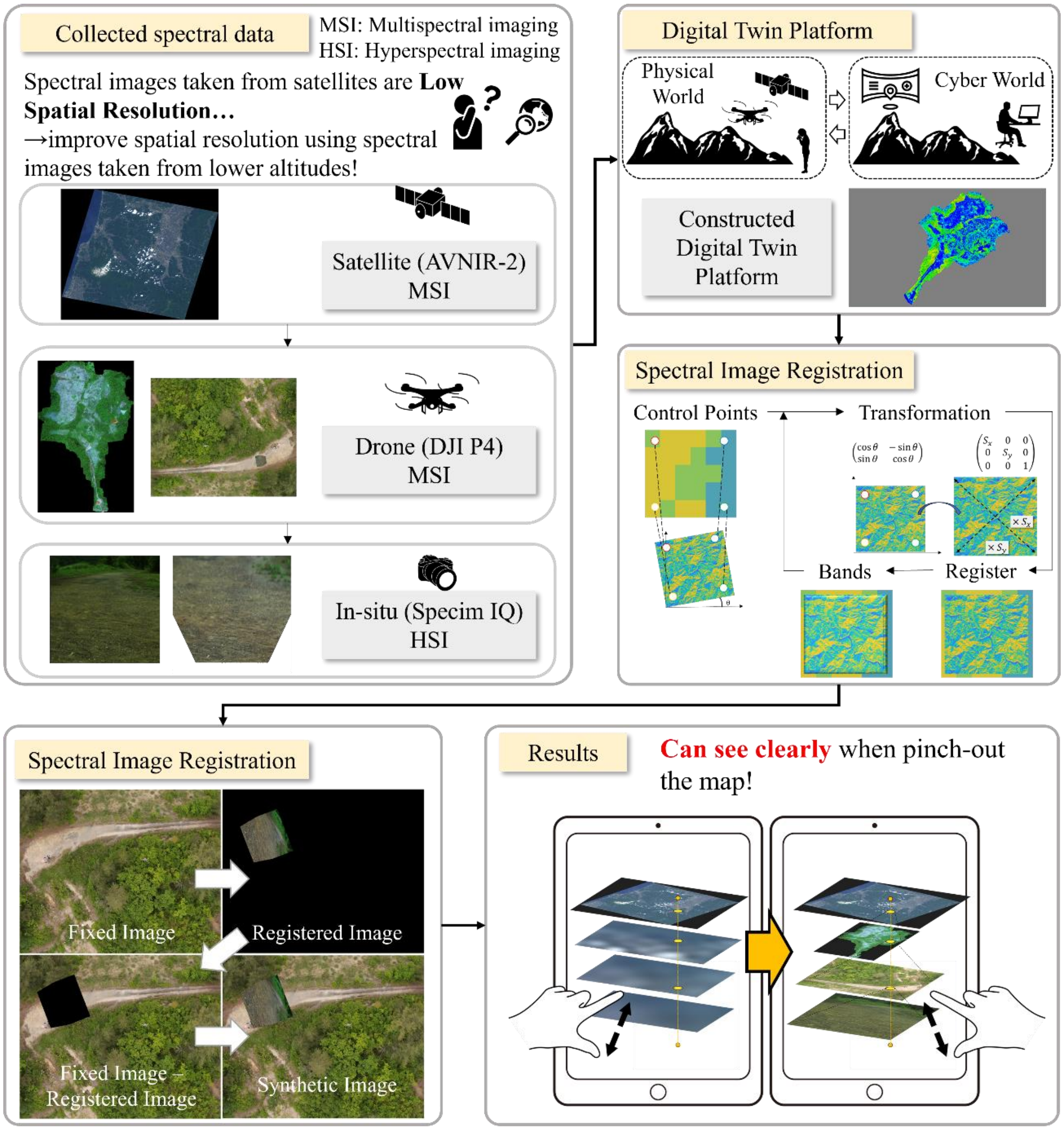

Figure 6 How the proposed system works.

3. Example of the proposed system configuration

The installation of the suggested system in an actual mining site is explained in this section. The proposed system is the subject of this concept paper. This section presents an actual experiment that looked at the suggested system. The experiment was completed in the field located in Akita Prefecture. Given the presence of a closed mine in this field and the continued discharge of acidic mine wastewater, the Japanese government agency has initiated a mine wastewater neutralization treatment program. This has led to concerns about the potential for soil contamination, prompting the consideration of investigating the feasibility of implementing this technology. This research field covers a large area, making conventional soil sampling difficult. To address this challenge, our objective is to conduct a comprehensive and detailed soil analysis by integrating satellite data and high-resolution drone data, which facilitate wide-area exploration. Previous studies have demonstrated the potential of hyperspectral imaging in identifying heavy metal minerals, and the application of this technology is anticipated to facilitate efficient investigation [31].

3.1.1. 3D Modeling

As shown in Figure 7, a three-dimensional model of the Mine was generated using Structure from Motion from images acquired by UAV. As a result, a digital twin platform was established, which provided the foundation for data gathering and analysis. Different data visualizations related to geographic mapping and analysis are depicted in the figure. There are four portions in the image, each displaying a distinct kind of data visualization. In the upper-left corner, there are four thousand spectral photos of a certain region. A vibrant 3D representation of the same geographic area's height levels is seen in the top-right corner. A color gradient that runs from blue to red indicates low to high elevation levels. A realistic portrayal of the terrain and plants can be found in the bottom-left section of the image, which showcases a detailed 3D model in RGB natural hues. Another 3D model with false color representations of the NDVI is shown in the bottom-right section. This NDVI 3D model is helpful for examining the density and health of vegetation. This platform allows for the analysis and display of spectral data acquired through the development of various advanced image registration techniques that are discussed in the next section. This allows for the cross-sectional processing of spectral data and can be useful mineral resources exploration as well.

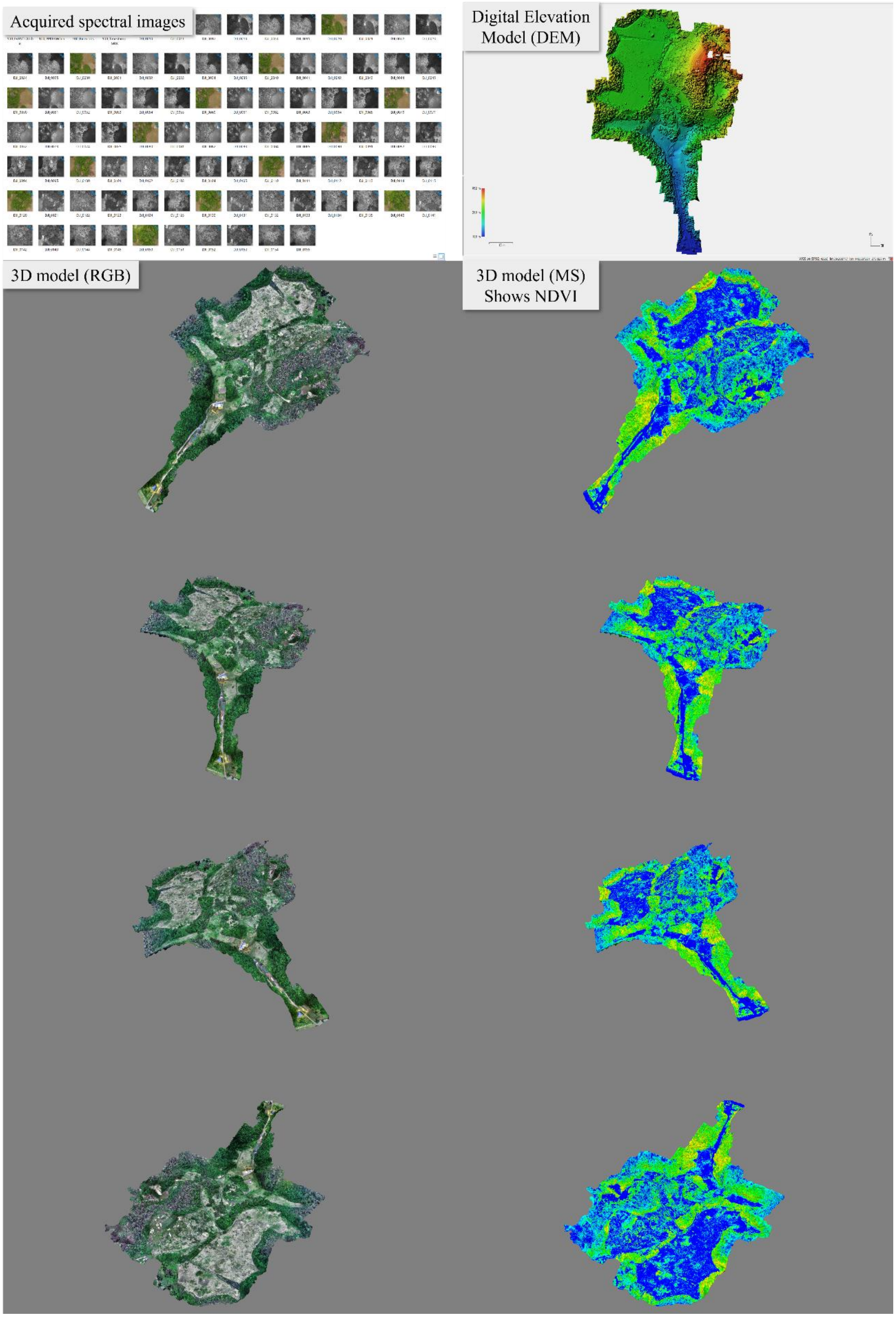

Figure 7 A constructed 3D model.

3.2. Bird’s eye transformation

The camera was angled twenty degrees with respect to the ground surface to achieve the bird's-eye view image modification. The outcomes are displayed in Figure 8, where the other images in the hyperspectral image are transformed using the same transformation matrix for the RGB image's bird's-eye view transformation. The procedure started with taking hyperspectral camera images in the designated area at a 20-degree angle while mounted on a tripod. Subsequently, the hyperspectral data was read and the bird's-eye view image was converted using a Python script. The only information that needed to be updated in the Python script before the code could be run was the angle information, as the script automatically gathers camera data. The RGB image underwent a bird's-eye view transformation first, and the other band images were then changed using the transformation matrix that was applied to the RGB image to create the hyperspectral data.

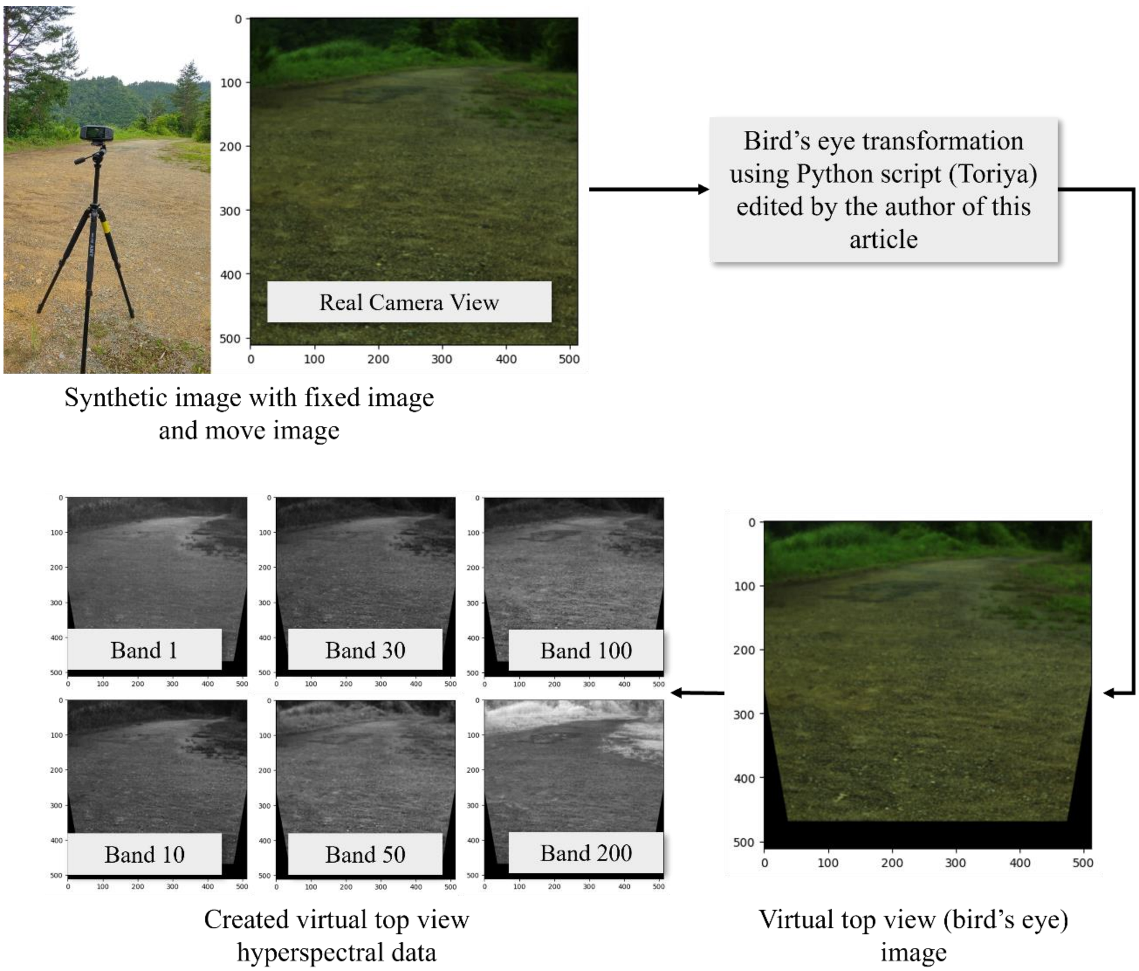

Figure 8 Results of the bird eye transformation for hyperspectral data.

3.2.1. Horizontal Registration

Instead of a single camera obtaining several band views, as seen in Figure 9, the drone cameras utilized in this work are configured so that each camera is assigned a specific band. In this case, there are six single-band cameras, although a total of five wavelengths and RGB images can be acquired. As a result, each wavelength has a slight variation in location in the horizontal direction while photographing the same object. It is not possible to acquire normal spectrum information if they are kept in the data cube exactly as they are. The horizontal misalignment was corrected by image registration. The same scene's spectral images were initially loaded, as seen in Figure 9, and detected feature points. After that, image registration was carried out using these images to produce a data cube with the horizontal misalignment fixed. Hyperspectral Viewer can be used to examine the generated data cube.

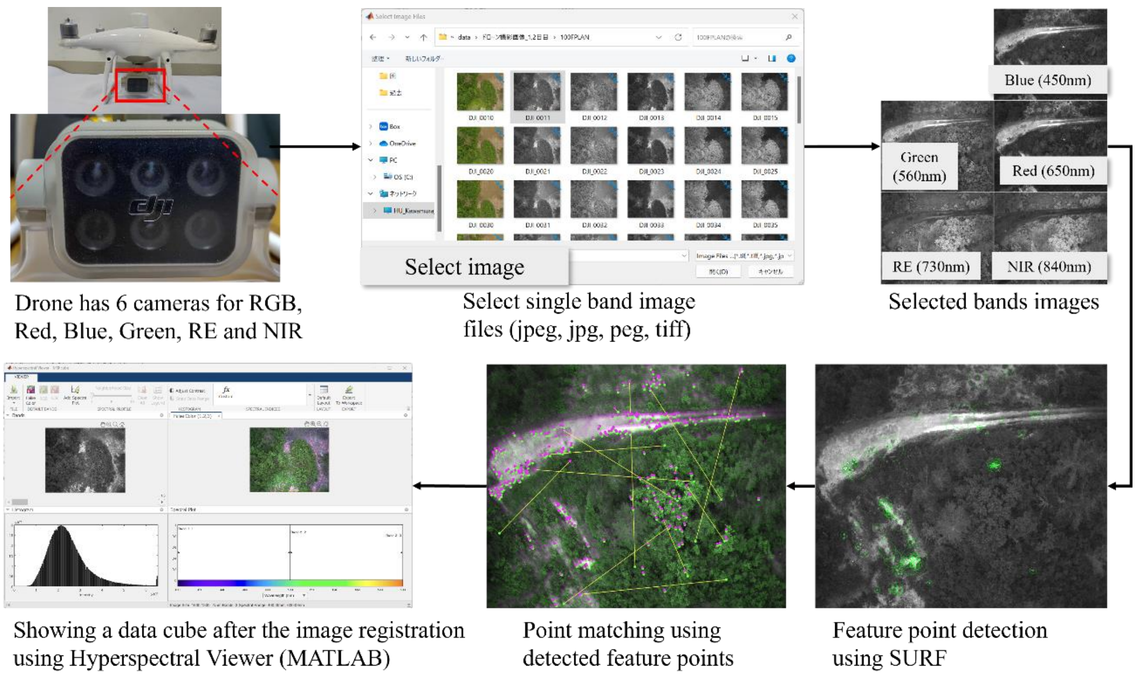

Figure 9 Image registration for drone camera images.

3.2.2. Vertical image misalignment

As seen in Figure 10, the images following the transformation to a bird's-eye perspective were manually selected feature points to coincide with images captured at a higher altitude. The feature points were extracted visually because automatic feature point extraction was not feasible due to the significant altitude difference. Figure 10 displays the image registration's outcome. The spatial resolution of the image acquired from low altitude was preserved while the image registration was computed to match the spectral image collected from higher altitude by fitting the move image to the corresponding coordinates on the fixed image. A conceptual diagram of the aligned spectral images is presented in Figure 11.

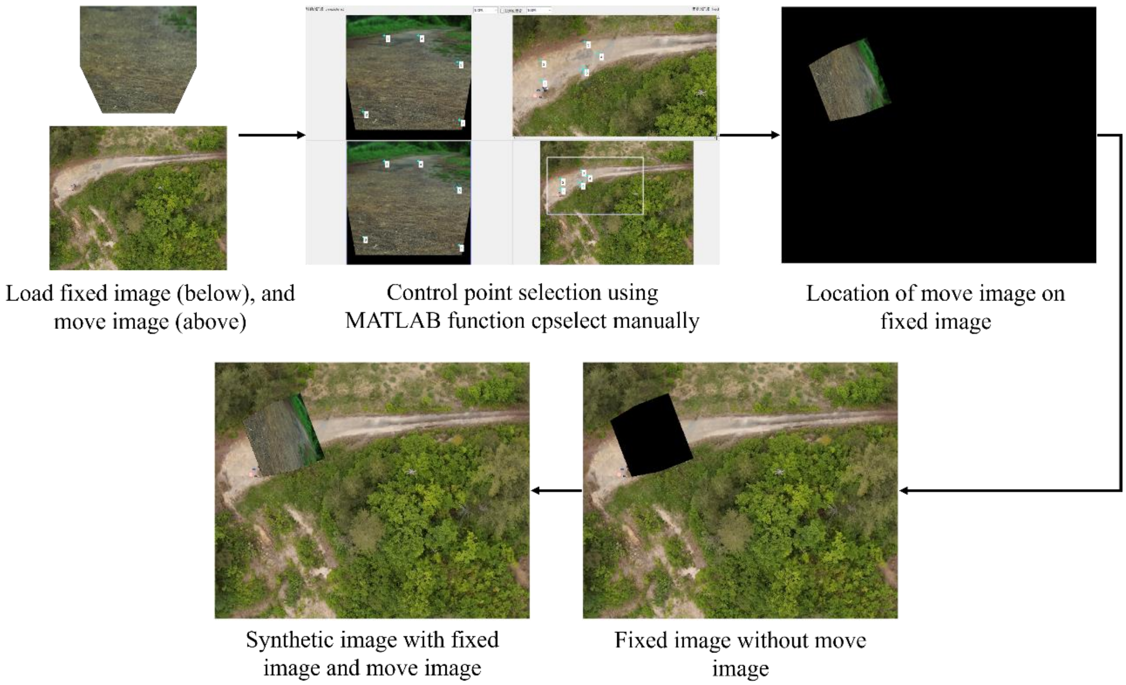

Figure 10 Control points selection shows as False RGB images.

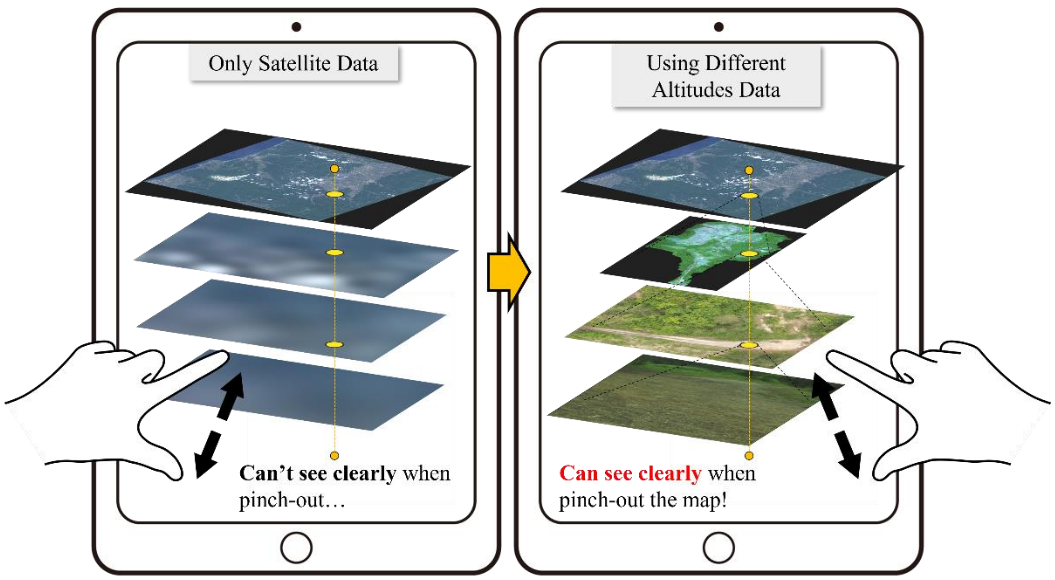

Figure 11 An overview of the result showed as False RGB images.

4. Limitations and Future Works

As this paper is concerned with the proposal of a registration technique for different altitude spectral images, the constructed spectral images have not been employed in the search for contaminated soil areas. In the future, we intend to combine this technique with machine learning in order to identify contaminated areas. Moreover, the proposed technology has the potential to be utilized for resource exploration. While currently constrained to mineral resources that are exposed on the surface of the Earth, it is anticipated that this technology can be employed to facilitate more comprehensive surveys than previously possible. To further these studies, it is essential to gather geological and mineralogical data. Subsequent studies will be conducted concurrently with the collection of this data and the investigation of the prospective applications of this technology.

5. Conclusions

This study investigated a spectral image registration method that may be able to address some of the issues related to remote sensing's lack of spatial resolution. The creation and administration process for this kind of system was also included in the study. Building a system that can examine spectral data obtained at different altitudes is the aim of this study. The closed mine in Akita Prefecture, Japan, was the subject of this investigation. The research was split into two sections: (1) system application through field research and lab testing; and (2) creation of various image registration methods. In the first section, 3D model of the mine site was produced from UAV data by employing Structure from Motion as the foundation for a digital twin. Part (2) involved the conversion of spectral data obtained from oblique angles during the field survey into bird's-eye view images, which were image registered with data obtained from higher altitudes to produce spectral data that was localized and had high resolution. We suggested a strategy for synchronizing spectral data from various altitudes on the same digital platform by merging the two terms mentioned above.

This work enhances the spatial resolution of spectral imagery obtained from various altitudes and permits cross-sectional analysis of spectral data groups from various altitudes, which was previously restricted to intermittent data linking. Heavy metal pollution of wasted minerals from mining development is a serious global-scale issue, and this study shows the potential to facilitate their environmental assessment.

6. Acknowledgments

The authors would like to thank Yokote City and Japan Organization for Metals and Energy Security (JOGMEC) for the research and providing the research field. We also thank the anonymous reviewers for their constructive comments on the manuscript.

Author Contributions: Conceptualization, N.O., Y.O., T.A., and Y.K.; Methodology, N.O.; Software, N.O., and H.T.; Validation, N.O.; Formal analysis, N.O. and A.G.; Investigation, N.O.,T.A., and A.G.; Resources, Y.K. and Y.O.; Data curation, N.O., H.T.; Writing—original draft, N.O.; Writing—review & editing, A.G., Y.O., and Y.K.; Visualization, N.O. and, H.T..; Supervision, Y.O.,T.A., and Y.K.; Project administration, Y.K.; Funding acquisition, Y.K. All authors have read and agreed to the published version of the manuscript.

Funding: This work is supported by JOGMEC and the Fukada Geological Institute under Fukada Field Research Grant.

Institutional Review Board Statement: Not applicable.

Informed Consent Statement: Not applicable.

Data Availability Statement: The data used in the study are available from the corresponding author upon reasonable request.

Conflicts of Interest: The authors declare no conflict of interest.

7. References

[1] J. A. Acosta, A. Faz, S. Martínez-Martínez, R. Zornoza, D. M. Carmona, and S. Kabas, "Multivariate statistical and GIS-based approach to evaluate heavy metals behavior in mine sites for future reclamation," *J Geochem Explor*, vol. 109, no. 1–3, pp. 8–17, Apr. 2011, doi: 10.1016/J.GEXPLO.2011.01.004.

[2] Z. Li, Z. Ma, T. J. van der Kuijp, Z. Yuan, and L. Huang, "A review of soil heavy metal pollution from mines in China: Pollution and health risk assessment," *Science of The Total Environment*, vol. 468–469, pp. 843–853, Jan. 2014, doi: 10.1016/J.SCITOTENV.2013.08.090.

[3] V. Balaram, "Rare earth elements: A review of applications, occurrence, exploration, analysis, recycling, and environmental impact," *Geoscience Frontiers*, vol. 10, no. 4, pp. 1285–1303, Jul. 2019, doi: 10.1016/J.GSF.2018.12.005.

[4] A. Akcil and S. Koldas, "Acid Mine Drainage (AMD): causes, treatment and case studies," *J Clean Prod*, vol. 14, no. 12–13, pp. 1139–1145, Jan. 2006, doi: 10.1016/J.JCLEPRO.2004.09.006.

[5] R. A. Schowengerdt, "Remote Sensing," *Remote Sensing: Models and Methods for Image Processing*, pp. 1–515, Jan. 2006, doi: 10.1016/B978-0-12-369407-2.X5000-1.

[6] F. A. Kruse, "Identification and mapping of minerals in drill core using hyperspectral image analysis of infrared reflectance spectra," *Int J Remote Sens*, vol. 17, no. 9, pp. 1623–1632, 1996, doi: 10.1080/01431169608948728.

[7] S. Peyghambari and Y. Zhang, "Hyperspectral remote sensing in lithological mapping, mineral exploration, and environmental geology: an updated review," *https://doi.org/10.1117/1.JRS.15.031501*, vol. 15, no. 3, p. 031501, Jul. 2021, doi: 10.1117/1.JRS.15.031501.

[8] P. Debba, F. J. A. Van Ruitenbeek, F. D. Van Der Meer, E. J. M. Carranza, and A. Stein, "Optimal field sampling for targeting minerals using hyperspectral data," *Remote Sens Environ*, vol. 99, no. 4, pp. 373–386, Dec. 2005, doi: 10.1016/J.RSE.2005.05.005.

[9] F. D. van der Meer *et al.*, "Multi- and hyperspectral geologic remote sensing: A review," *International Journal of Applied Earth Observation and Geoinformation*, vol. 14, no. 1, pp. 112–128, 2012, doi: https://doi.org/10.1016/j.jag.2011.08.002.

[10] J. Jia *et al.*, "Tradeoffs in the Spatial and Spectral Resolution of Airborne Hyperspectral Imaging Systems: A Crop Identification Case Study," *IEEE Transactions on Geoscience and Remote Sensing*, vol. 60, 2022, doi: 10.1109/TGRS.2021.3096999.

[11] P. Raj and C. Surianarayanan, "Chapter Twelve - Digital twin: The industry use cases," in *Advances in Computers*, vol. 117, no. 1, P. Raj and P. Evangeline, Eds., Elsevier, 2020, pp. 285–320. doi: https://doi.org/10.1016/bs.adcom.2019.09.006.

[12] N. Yokoya, "Resolution Enhancement of Hyperspectral Imagery," *Journal of The Remote Sensing Society of Japan*, vol. 38, no. 2, pp. 105–110, 2018, doi: 10.11440/rssj.38.105.

[13] T. Akgun, Y. Altunbasak, and R. M. Mersereau, "Super-resolution reconstruction of hyperspectral images," *IEEE Transactions on Image Processing*, vol. 14, no. 11, pp. 1860–1875, Nov. 2005, doi: 10.1109/TIP.2005.854479.

[14] P. V. Arun, K. M. Buddhiraju, A. Porwal, and J. Chanussot, "CNN-Based Super-Resolution of Hyperspectral Images," *IEEE Transactions on Geoscience and Remote Sensing*, vol. 58, no. 9, pp. 6106–6121, Sep. 2020, doi: 10.1109/TGRS.2020.2973370.

[15] Y. Li, J. Hu, X. Zhao, W. Xie, and J. J. Li, "Hyperspectral image super-resolution using deep convolutional neural network," *Neurocomputing*, vol. 266, pp. 29–41, Nov. 2017, doi: 10.1016/J.NEUCOM.2017.05.024.

[16] L. Zhang, J. Nie, W. Wei, Y. Li, and Y. Zhang, "Deep Blind Hyperspectral Image Super-Resolution," *IEEE Trans Neural Netw Learn Syst*, vol. 32, no. 6, pp. 2388–2400, Jun. 2021, doi: 10.1109/TNNLS.2020.3005234.

[17] W. Dong, C. Zhou, F. Wu, J. Wu, G. Shi, and X. Li, "Model-Guided Deep Hyperspectral Image Super-Resolution," *IEEE Transactions on Image Processing*, vol. 30, pp. 5754–5768, 2021, doi: 10.1109/TIP.2021.3078058.

[18] X. Xu, Y. Zhong, L. Zhang, and H. Zhang, "Sub-pixel mapping based on a MAP model with multiple shifted hyperspectral imagery," *IEEE J Sel Top Appl Earth Obs Remote Sens*, vol. 6, no. 2, pp. 580–593, 2013, doi: 10.1109/JSTARS.2012.2227246.

[19] X. Xu, Y. Zhong, L. Zhang, and H. Zhang, "Sub-pixel mapping based on a MAP model with multiple shifted hyperspectral imagery," *IEEE J Sel Top Appl Earth Obs Remote Sens*, vol. 6, no. 2, pp. 580–593, 2013, doi: 10.1109/JSTARS.2012.2227246.

[20] P. V. Arun, K. M. Buddhiraju, and A. Porwal, “CNN based sub-pixel mapping for hyperspectral images,” *Neurocomputing*, vol. 311, pp. 51–64, Oct. 2018, doi: 10.1016/J.NEUCOM.2018.05.051.
[21] F. Fang, F. Li, C. Shen, and G. Zhang, “A variational approach for pan-sharpening,” *IEEE Transactions on Image Processing*, vol. 22, no. 7, pp. 2822–2834, 2013, doi: 10.1109/TIP.2013.2258355.
[22] N. Yokoya, C. Grohnfeldt, and J. Chanussot, “Hyperspectral and multispectral data fusion: A comparative review of the recent literature,” *IEEE Geosci Remote Sens Mag*, vol. 5, no. 2, pp. 29–56, Jun. 2017, doi: 10.1109/MGRS.2016.2637824.
[23] G. Vivone *et al.*, “A critical comparison among pansharpening algorithms,” *IEEE Transactions on Geoscience and Remote Sensing*, vol. 53, no. 5, pp. 2565–2586, May 2015, doi: 10.1109/TGRS.2014.2361734.
[24] L. Loncan *et al.*, “Hyperspectral Pansharpening: A Review,” *IEEE Geosci Remote Sens Mag*, vol. 3, no. 3, pp. 27–46, Sep. 2015, doi: 10.1109/MGRS.2015.2440094.
[25] N. Yokoya, C. Grohnfeldt, and J. Chanussot, “Hyperspectral and multispectral data fusion: A comparative review of the recent literature,” *IEEE Geosci Remote Sens Mag*, vol. 5, no. 2, pp. 29–56, Jun. 2017, doi: 10.1109/MGRS.2016.2637824.
[26] M. Marconcini *et al.*, “Digital Twin Technology Challenges and Applications: A Comprehensive Review,” *Remote. Sens.*, vol. 14, p. 1335, 2022, [Online]. Available: https://api.semanticscholar.org/CorpusID:266022735
[27] A. Rasheed, O. San, and T. Kvamsdal, “Digital Twin: Values, Challenges and Enablers From a Modeling Perspective,” *IEEE Access*, vol. 8, pp. 21980–22012, 2019, [Online]. Available: https://api.semanticscholar.org/CorpusID:211060692
[28] K.-H. G. Bae *et al.*, “DIGITAL TWINS IN SIMULATIVE APPLICATIONS : A TAXONOMY,” 2020. [Online]. Available: https://api.semanticscholar.org/CorpusID:230125766
[29] H. Toriya, “Correspondence Point Search Method between Images Taken at Different Altitudes for Spatiotemporal Resolution Improvement of Geographic Information Systems,” *Doctoral Thesis, Graduate School of Systems and Information Engineering, University of Tsukuba*, p. 78, 2021.
[30] H. Toriya *et al.*, “Mutual superimposing of SAR and ground-level shooting images mediated by intermediate multi-altitude images,” *Array*, vol. 12, p. 100102, Dec. 2021, doi: 10.1016/J.ARRAY.2021.100102.
[31] N. Okada *et al.*, “Optimizing multi-spectral ore sorting incorporating wavelength selection utilizing neighborhood component analysis for effective arsenic mineral detection,” *Scientific Reports 2024 14:1*, vol. 14, no. 1, pp. 1–21, May 2024, doi: 10.1038/s41598-024-62166-0.

List of Figures

List of Tables